

## In Situ Measure of Interfacial Tensions in Ternary and Quaternary Immiscible Polymer Blends Demonstrating Partial Wetting

Nick Virgilio,<sup>†</sup> Patrick Desjardins,<sup>‡</sup> Gilles L'Espérance,<sup>§</sup> and Basil D. Favis<sup>\*†</sup>

<sup>†</sup>*Centre de Recherche En Plasturgie Et Composites (CREPEC), Department of Chemical Engineering and*

<sup>‡</sup>*Regroupement Québécois sur les Matériaux de Pointe (RQMP), Department of Engineering Physics and*

<sup>§</sup>*Center for Characterization and Microscopy of Materials (CM)<sup>2</sup>, École Polytechnique de Montréal, Montréal, Québec H3C 3A7, Canada*

Received March 13, 2009; Revised Manuscript Received June 27, 2009

**ABSTRACT:** This article reports on the use of the Neumann triangle method combined with a focused ion beam sample preparation technique and atomic force microscopy (NT-FIB-AFM) to measure interfacial tension ratios in partially wetted ternary and quaternary immiscible polymer blends prepared by melt processing. It is shown that PS/PP/HDPE, PS/PCL/PP, PLLA/PCL/PS, PMMA/PS/PP, and a quaternary blend system comprised of HDPE/PP/PS/PMMA all display a partial wetting morphology with a three-phase line of contact and that the interfacial tension ratios obtained by the NT-FIB-AFM approach compare well with results obtained by the classical breaking thread method. The HDPE/PP/PS/PMMA quaternary blend, in particular, is quite unique and displays a partial wetting morphology with spectacular PS/PMMA composite droplets located at the HDPE/PP interface. Furthermore, all of the above data generated for the ternary and quaternary systems also satisfy the Laplace equation. When 1% of an SEB diblock copolymer is added to the PS/PP/HDPE system, the Neumann triangle method reveals that the PS/HDPE interfacial tension decreases from  $4.2 \pm 0.6$  to  $3.3 \pm 0.4$  mN/m, with an estimated apparent areal density of  $0.19 \pm 0.07$  molecule/nm<sup>2</sup> of copolymer at the PS/HDPE interface. The results presented in this paper show that it is possible to generate complex morphologies demonstrating partial wetting for a wide range of polymer blend systems with a relatively simple experimental approach. Furthermore, it allows the measurement of the interfacial tension ratios of a matrix-dispersed phase blend system examined in situ after melt processing. The apparent areal density of a copolymer interfacial modifier can also be estimated. This is an important result, since it is still a challenge to measure the variation of the interfacial tension as a function of the copolymer areal density in multiphase polymer blends.

### 1. Introduction

The controlled formation of complex microstructured multiphase materials is an important area of research in advanced materials science.<sup>1–4</sup> In immiscible multiphase polymer blends prepared by melt processing, morphology development is in part controlled by the interfacial properties between the phases, more specifically by the interfacial tensions between the components. Although a good number of methods available to measure the interfacial tension between two immiscible homopolymers have been reviewed recently,<sup>5,6</sup> virtually all of these techniques require dedicated ex-situ experimental setup, and most cannot be used directly on melt-processed blends. In binary blends having a matrix/dispersed phase morphology, interfacial tensions calculated with rheological measurements have yielded very interesting results for uncompatibilized and compatibilized systems.<sup>7–16</sup> However, the mathematical formalism is relatively heavy, the experimental conditions can be quite restrictive since the droplets diameter must remain uniform and constant in size during measurements, and the addition of a compatibilizer complicates the analysis even more due to the copolymer concentration gradients that develop during flow at the interface.

No work to date has measured the interfacial tension in situ in polymer blend systems after melt mixing by simply using the blends' morphological features. Furthermore, the effect of interfacial modification on complex morphology formation in

ternary and quaternary blends has only been marginally addressed in the literature to date.<sup>17–21</sup> Ternary immiscible homopolymer blends have a definite potential to address these topics. The relative positions of the A, B, and C phases within the blend can be predicted by using a set of three spreading coefficients  $\lambda_{ijk}$ .<sup>22–25</sup>

$$\lambda_{ABC} = \gamma_{AC} - (\gamma_{AB} + \gamma_{BC}) \quad (1a)$$

$$\lambda_{ACB} = \gamma_{AB} - (\gamma_{AC} + \gamma_{BC}) \quad (1b)$$

$$\lambda_{BAC} = \gamma_{BC} - (\gamma_{AB} + \gamma_{AC}) \quad (1c)$$

where the  $\gamma$  values are the interfacial tensions between the different phases. Each spreading coefficient gives the tendency of one phase to spread and form a continuous layer at the interface of the other two. For example,  $\lambda_{ABC}$  gives the tendency of phase B to spread and form a layer at the interface of phases A and C. If phase B spreads between A and C, it is said that phase B completely wets the AC interface and the corresponding spreading coefficient will be positive, while the other two will be negative. Following this analysis, four types of microstructures can result depending on the signs of the spreading coefficients. Figure 1a–c shows the three possible morphologies corresponding to complete wetting. In each case, the relevant spreading coefficient is positive, while the other two are negative. The fourth possible morphology appears when the three spreading coefficients are negative. In that case, none of the three polymers spreads and forms a complete layer at the interface of the other two. Instead, all three polymers meet along a common line of

\*Corresponding author: e-mail basil.favis@polymtl.ca; Tel +1 514 340-4711 ext 4527; Fax +1 514 340-4159.

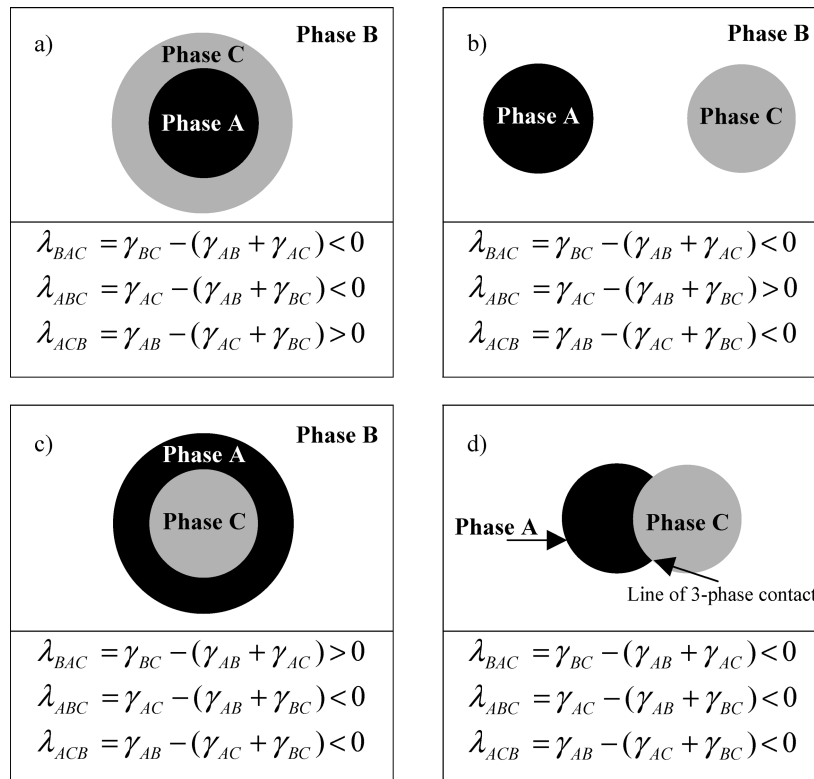


**Figure 1.** Possible morphologies in a ternary system composed of two minor phases A and C (in black and gray) and one major phase B (white), as predicted by the signs of the spreading coefficients. From (a) to (c), morphologies displaying complete wetting, in which phases C, B, and A respectively wet the AB, AC, and BC interfaces. In (d), morphology exhibiting partial wetting, in which none of the phases locates between the other two, resulting in a 3-phase line of contact.<sup>24</sup>

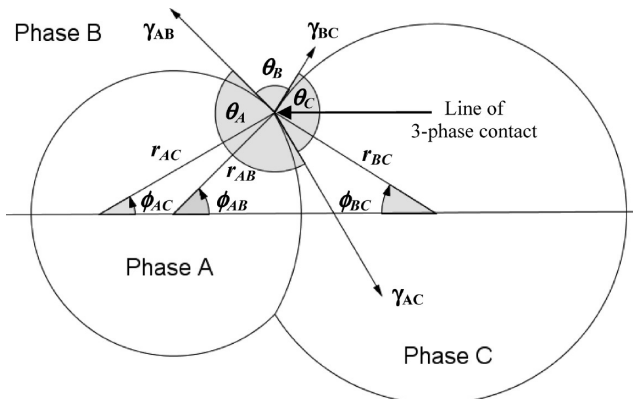


**Figure 2.** Geometrical parameters of a ternary blend displaying partial wetting.<sup>24</sup>  $\theta_A$ ,  $\theta_B$ , and  $\theta_C$  are the contact angles between the phases at the line of 3-phase contact, and  $\gamma_{AB}$ ,  $\gamma_{AC}$ , and  $\gamma_{BC}$  are the three interfacial tensions. The radius of curvature  $r_{ij}$  of the interfaces and the angles  $\phi_{ij}$  are characteristic geometrical parameters of this microstructure.

contact, called the 3-phase line. In that case, each polymer phase is adjacent to the other two, resulting in a partial wetting type of morphology, as shown in Figure 1d.

Torza and Mason<sup>24,25</sup> have calculated the equilibrium geometry of contact between three immiscible phases displaying partial wetting when the effect of the 3-phase line of tension is negligible (Figure 2). For this type of microstructure, the equilibrium is reached when both the Laplace and the Neumann equations are satisfied.<sup>24–28</sup> The Laplace equation relates the pressure difference across a curved interface to the interfacial tension and the curvature of the interface. For partial wetting, three Laplace equations have to be satisfied, since there are three distinct

interfaces AB, AC, and BC:

$$p_A - p_B = \frac{2\gamma_{AB}}{r_{AB}} \quad (2a)$$

$$p_A - p_C = \frac{2\gamma_{AC}}{r_{AC}} \quad (2b)$$

$$p_C - p_B = \frac{2\gamma_{BC}}{r_{BC}} \quad (2c)$$

where  $p_A$ ,  $p_B$ , and  $p_C$  are the internal bulk pressures of the homopolymer phases and  $r_{AB}$ ,  $r_{AC}$ , and  $r_{BC}$  are the radius of curvature of the corresponding interfaces. Furthermore, the three interfacial tensions act perpendicularly to the line of 3-phase contact and equilibrium along it is reached when the vector sum of the three interfacial tensions equals zero:

$$\vec{\gamma}_{AB} + \vec{\gamma}_{AC} + \vec{\gamma}_{BC} = \vec{0} \quad (3)$$

This equation corresponds to the simplified form of the Neumann triangle relation.<sup>26–29</sup> At equilibrium, the three tensions (or phases) define three contact angles  $\theta_i$  from which one can calculate the three interfacial tension ratios  $\Gamma_A$ ,  $\Gamma_B$ , and  $\Gamma_C$ .<sup>29</sup>

$$\Gamma_A = \frac{\gamma_{AC}}{\gamma_{AB}} = \frac{\sin \theta_B}{\sin \theta_C} \quad (4a)$$

$$\Gamma_B = \frac{\gamma_{BC}}{\gamma_{AB}} = \frac{\sin \theta_A}{\sin \theta_C} \quad (4b)$$

$$\Gamma_C = \frac{\gamma_{BC}}{\gamma_{AC}} = \frac{\sin \theta_A}{\sin \theta_B} \quad (4c)$$

In order to be able to use the Neumann triangle method, a ternary blend must display at equilibrium a partial wetting type of morphology in which a 3-phase line of contact is formed. As indicated above, such morphologies are predicted when all three

spreading coefficients are negative. It is afterward possible to obtain the absolute values of the interfacial tensions if at least one tension out of the three has been measured with another method, such as the breaking thread.

Although complete wetting has been reported in a certain number of articles,<sup>20,21,30–34</sup> very few have reported partial wetting in ternary polymer blends.<sup>17,19,35</sup> In a recent article,<sup>36</sup> we showed that PS/PP/HDPE ternary blends exhibit partial wetting and that it is possible to control the complete/partial wetting behavior by the addition of a suitably chosen interfacial agent. This led to the formation of a striking new type of morphology in which the PS droplets are exclusively located at the HDPE/PP interface, forming a very dense array similar to a Pickering emulsion or a bijel. Horiuchi et al.<sup>19</sup> observed partial wetting in ternary polymer blends of polyamide-6/polycarbonate/polystyrene (PA6/PC/PS) and polyamide-6/polycarbonate/styrene-(ethylene-butylene)-styrene triblock copolymer (PA6/PC/SEBS). They induced a morphological transition from partial to complete wetting by using PS and SEBS grafted with maleic anhydride (PS-*g*-MA and SEBS-*g*-MA). By reacting at the interface with the PA6, a copolymer was formed, lowering the PS/PA6 or SEBS/PA6 interfacial tension and inducing the complete encapsulation of PC by PS or SEBS.

In addition, a few articles report the use of the Neumann triangle method to measure interfacial tensions between different polymer pairs in a layered geometry. Hyun et al.,<sup>37</sup> Kim et al.,<sup>38</sup> and Zhang et al.<sup>39</sup> have measured interfacial tensions in ternary combinations of polypropylene/polystyrene/poly(methyl methacrylate) (PP/PS/PMMA) and polystyrene/poly(butylene terephthalate)/poly(methyl methacrylate) (PS/PBT/PMMA) with and without the addition of a small amount of poly(styrene-*co*-glycidyl methacrylate) (PS-GMA). For this last case, the PS-GMA reacts with the PBT to form a PBT-*graft*-PS copolymer, lowering the PS-PBT interfacial tension. This modification significantly changed the contact angles between the phases, confirming the sensitivity of the Neumann triangle method to measure variations of the interfacial tensions.

The objectives of this article are to investigate the applicability of the Neumann triangle method and Laplace equation, combined with a focused ion beam sample preparation and atomic force microscopy analysis,<sup>40</sup> in measuring interfacial tension ratios in situ in ternary and quaternary immiscible homopolymer blends demonstrating partial wetting and prepared by melt processing. The effect of an interfacial modifier on the interfacial tension ratios is also considered.

## 2. Experimental Methods

**2.1. Materials.** Seven homopolymers and one diblock copolymer were used. A barefoot resin of high-density polyethylene, HDPE 3000, was supplied by Petromont. Polypropylene PP PD702 was obtained from Basell and polystyrene PS 615APR from Americas Styrenics. Poly(methyl methacrylate) 200336 (PMMA1) was supplied by Aldrich and used for the prepared blends, while PMMA IRD-2 (PMMA2) was from Rohm and Haas and was used for the breaking thread measurements. Poly( $\epsilon$ -caprolactone) (PCL 6800) and a poly(L-lactide) (PLLA) were from Solvay-Interox and Boehringer-Ingelheim, respectively. SEB CAP4741, a commercial 1,4-hydrogenated styrene-*block*-(ethylene-butylene) diblock copolymer, was supplied by Shell. The materials characteristics are listed in Table 1.

**2.2. Rheology.** The rheological characterization of the homopolymers was performed using a SR-5000 constant stress rheometer from Rheometrics operated in the oscillatory mode. A parallel plate geometry with a gap of 1.0 mm under a nitrogen atmosphere was employed. The stability of the pure materials was measured at 1 Hz and 200 °C. Stress sweeps were performed

**Table 1. Materials Characteristics**

polymers	$M_n \times 10^{-3}{}^a$ (g/mol)	melt index <sup>a</sup> (g/10 min) (ASTM)	$\eta^* \times 10^{-3}$ (Pa s) at 200 °C and 25 s <sup>-1</sup>	$\eta_0 \times 10^{-3}$ (Pa s) at 200 °C
HDPE		8.1	0.42	1.1
PP	89	35.0	0.27	0.71
PS	95 ( $M_w$ )	14.0	0.49	4.04
PMMA 1 <sup>b</sup>	7.8			
PMMA 2 <sup>b</sup>	46.8	5.5	7.0	35.8
PLLA <sup>c</sup>			5.0	20
PCL	69	3.0	1.0	1.1
SEB	21.0- <i>b</i> -46.0			

<sup>a</sup> Obtained from suppliers. <sup>b</sup> Refs 31 and 32,  $M_n$  determined by GPC. <sup>c</sup> Reference 64.

to identify the region of linear viscoelasticity of the materials. Frequency sweeps were used to obtain the zero-shear viscosity of the pure homopolymers, which has been approximated using the modulus of the complex viscosity at low frequencies when the plateau value was reached. In all cases, the loss angles were sufficiently near 90° to consider the homopolymers as nonelastic Newtonian fluids. The rheological properties are reported in Table 1.

**2.3. Blend Preparation.** The blends and the volume fractions of each constituent are listed in Table 2. Blends 1, 2, and 4 were prepared in a Plasti-Corder Digi-System internal mixer from C. W. Brabender Instruments Inc. at 200 °C and 50 rpm for 8 min under a constant nitrogen flow. The PLLA/PCL/PS blend (blend 3) was mixed for 7 min.

The PS/PP/HDPE blend modified with 1% SEB copolymer (based on PS content, blend 5) was prepared in two steps to maximize the migration of the SEB copolymer to the HDPE/PS interface. Pure PS was initially blended with 1% SEB (based on the PS volume content) at 180 °C and 50 rpm for 5 min under a constant nitrogen flow and then quenched in cold water. The ternary blend was subsequently prepared with the required amount of PS + SEB at 200 °C and 50 rpm for 8 min under a constant nitrogen flow.

A small amount (0.2 wt %) of Irganox B-225 from Ciba-Geigy was added to all blends in order to prevent thermal degradation. After melt processing, the blends were first quenched in cold water to freeze-in the morphology.

**2.4. Breaking Thread for Interfacial Tension Measurement.** In order to obtain reference values of the various interfacial tensions, all binary blend permutations were measured using the breaking thread method (BT),<sup>41,42</sup> except when specified. For the  $\gamma_{PS/HDPE}$ ,  $\gamma_{PS/PP}$ , and  $\gamma_{PS/PCL}$  interfacial tension measurements, PS threads with diameters ranging from 30 to 60  $\mu\text{m}$  were first annealed at 120 °C for 24 h under vacuum to remove the residual stress. They were subsequently sandwiched between HDPE, PP, or PCL films, respectively. For the  $\gamma_{PP/HDPE}$  interfacial tension measurement, PP threads were sandwiched between HDPE films. For the  $\gamma_{PMMA2/PP}$  tension, PMMA2 threads with diameters ranging from 30 to 60  $\mu\text{m}$  were first annealed at 100 °C under vacuum to remove the residual stress and were then sandwiched between PP films. Finally,  $\gamma_{PCL/PP}$  was measured by sandwiching PP fibers between PCL films. Measurements were performed at 200 °C using an Optiphot-2 microscope from Nikon and a Mettler FP-82HT hot stage connected to a Mettler FP-90 central processor. Digital images were captured and analyzed using Streampix v.III and Visilog v.6.3 software applications, provided by Norpix. The interfacial tensions  $\gamma$  are obtained by using the following equation:

$$\gamma = \frac{q\eta_m D_0}{\Omega} \quad (5)$$

where  $q$  values are the slopes in the data shown in Figure 3,  $\eta_m$  is the viscosity of the polymer films used for the experiment,  $D_0$  is

Table 2. Ternary and Quaternary Blends and Their Compositions

blend	polymer A composition (vol %)	polymer B composition (vol %)	polymer C composition (vol %)	polymer D composition (vol %)
1	PS 10	PP 45	HDPE 45	
2	PS 4	PCL 53	PP 43	
3	PLLA 10	PCL 45	PS 45	
4	PMMA 5	PP 45	PS 5	HDPE 45
5	PS 10	PP 45	HDPE 45	SEB 1 g/100 mL PS

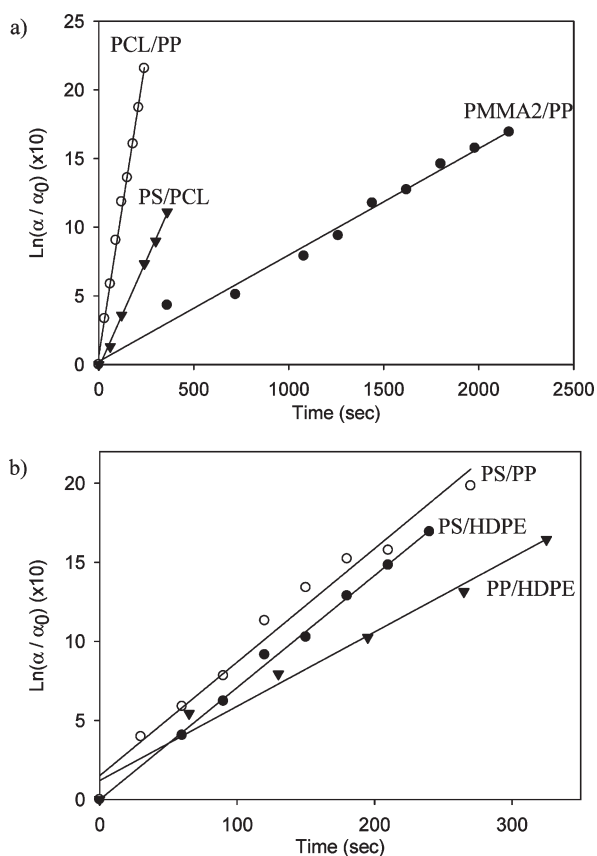


**Figure 3.** Typical examples of breaking thread results used to calculate the interfacial tensions for (a) PMMA2/PP, PCL/PP, and PS/PCL pairs and (b) PS/HDPE, PS/PP, and PP/HDPE pairs.

the initial fiber diameter, and  $\Omega$  is a tabulated function given in Tomotika's article.<sup>41</sup> Relative distortion amplitudes  $\alpha/\alpha_0$  of the fibers, where  $\alpha_0$  is the distortion amplitude  $(D_{\max} - D_{\min})_{t=t_0}$  at the beginning of the measurements and  $\alpha$  is the distortion amplitude  $(D_{\max} - D_{\min})_t$  at time  $t$ , are shown in Figure 3 for some homopolymer pairs. Between 4 and 10 measurements were obtained for each tension. Since the  $\gamma_{PP/HDPE}$  tension is particularly more difficult to measure using this technique, only two values were considered reliable. The polymers were initially blended with Irganox B-225 (0.2 wt %) to prevent thermal degradation during the experiment. The average interfacial tensions and standard deviations  $\sigma$ , along with the number of measurements  $N$ , are reported in Table 3, and their relative magnitudes are generally comparable with other reported results when available,<sup>17,18,20,21,31–33,43,44</sup> except for the PS/PCL tension. However, only one reference reporting this value

Table 3. Interfacial Tensions Obtained by the Breaking Thread Method

polymer pairs	no. of measurements $N$	interfacial tensions $\gamma$ (mN/m)
PS/HDPE	5	$4.9 \pm 0.6$
PS/PP	5	$3.5 \pm 0.2$
PP/HDPE	2	$1.9 \pm 0.5$
PMMA/HDPE		$8.6 \pm 0.9^a$
PMMA/PP	4	$5.7 \pm 1.0$
PMMA/PS		$2.4 \pm 0.3^a$
PCL/PP	12	$5.8 \pm 1.0$
PS/PCL	7	$2.4 \pm 0.6$
PLLA/PS		$5.8 \pm 0.6^b$
PLLA/PCL		$c$

<sup>a</sup> From ref 31. <sup>b</sup> Average from refs 64 and 65. <sup>c</sup> Not measured due to degradation issue.

seems to exist in the literature.<sup>45</sup> The spreading coefficient values for each blend are reported in Table 4.

**2.5. Scanning Electron Microscope Observations.** Samples were initially cryogenically microtomed using a Leica RM2165 microtome equipped with a LN21 cooling system. For SEM observations, the PS phase was subsequently extracted at room temperature for 3 days using cyclohexane as a selective solvent and then dried for 2 days at 60 °C under vacuum in an oven. The samples were then coated with a gold–palladium layer by plasma sputtering. SEM observations were conducted using a JEOL JSM 840 scanning electron microscope operated at 10 kV and  $6 \times 10^{-11}$  A.

**2.6. Focused Ion Beam Sample Preparation and Atomic Force Microscopy Analysis.** The combination of focused ion beam (FIB) and AFM has been shown in a previous article<sup>40</sup> to result in an outstanding contrast between the phases for morphology analysis. Before the FIB/AFM procedure, samples from each blend were annealed at 200 °C under quiescent conditions: 5 min for blend 3 and 30 min for the others. They were subsequently plunged into cold water to freeze-in the morphology. This rapid quench approach cools the samples in a matter of seconds. Samples for the focused ion beam (FIB) preparation were then cryogenically microtomed, and a gold–palladium layer was deposited on the samples by plasma sputtering. Finally, the surface of the specimens was prepared with the focused ion beam. The FIB surface etching was performed using a Hitachi 2000A Ga<sup>+</sup> focused ion beam operated at 30 keV and 3 nA, with an etching window of  $120 \times 10 \mu\text{m}^2$  and a dwelling time of 3  $\mu\text{s}$ . The etched surface was then analyzed with an AFM in tapping mode using a Dimension 3100 scanning probe microscope from Veeco Instruments equipped with a Nanoscope IVa control module. Tips model PPP-NCH-W from Nanosensors, with a resonance frequency of 204–497 kHz, a force constant of 10–130 N/m, length and width of  $125 \pm 10 \mu\text{m}$  and  $30 \pm 7.5 \mu\text{m}$ , tip height of 10–15  $\mu\text{m}$ , and radius < 10 nm, were used. Topographic

**Table 4. Spreading Coefficients Based on the Breaking Thread Measurements<sup>a</sup>**

ternary polymer blend		spreading coefficients $\lambda$ (mN/m) (based on breaking thread)	
PS/PP/HDPE	$\lambda_{\text{HDPE/PS/PP}}$	$-6.5 \pm 1.3$	partial wetting
	$\lambda_{\text{HDPE/PP/PS}}$	$-0.5 \pm 1.3$	
	$\lambda_{\text{PP/HDPE/PS}}$	$-3.3 \pm 1.3$	
PS/PCL/PP	$\lambda_{\text{PP/PS/PCL}}$	$-0.1 \pm 1.8$	partial wetting
	$\lambda_{\text{PP/PCL/PS}}$	$-4.7 \pm 1.8$	
	$\lambda_{\text{PCL/PP/PS}}$	$-6.3 \pm 1.8$	
PMMA/PP/PS	$\lambda_{\text{PP/PMMA/PS}}$	$-4.6 \pm 1.5$	partial wetting
	$\lambda_{\text{PP/PS/PMMA}}$	$-0.2 \pm 1.5$	
	$\lambda_{\text{PS/PP/PMMA}}$	$-6.8 \pm 1.5$	
HDPE/PS/PMMA	$\lambda_{\text{HDPE/PMMA/PS}}$	$-6.1 \pm 1.8$	complete wetting PS spreads between HDPE and PMMA
	$\lambda_{\text{HDPE/PS/PMMA}}$	$1.3 \pm 1.8$	
	$\lambda_{\text{PS/HDPE/PMMA}}$	$-11.1 \pm 1.8$	
PMMA/PP/HDPE	$\lambda_{\text{HDPE/PMMA/PP}}$	$-11.5 \pm 2.1$	complete wetting PP spreads between HDPE and PMMA
	$\lambda_{\text{HDPE/PP/PMMA}}$	$1.9 \pm 2.1$	
	$\lambda_{\text{PMMA/HDPE/PP}}$	$-5.7 \pm 2.1$	

<sup>a</sup>The coefficients in italics indicate that complete wetting is expected in these ternary systems.

(height) images were subsequently treated with the AFM software to remove the effects caused by inclination of the samples and the curtain effect produced by FIB surface preparation.

**2.7. The Neumann Triangle Method for Interfacial Tension Analysis.** *2.7.1. Method.* The Neumann triangle method (NT) was applied on the FIB-AFM images obtained from the blends previously annealed at 200 °C and subsequently quenched in cold water. This approach will be designated as the FIB-AFM-NT method or NT method. For each blend, the homopolymers used for the Neumann triangle analysis are identified by the letters A, B, and C (Table 2). For example, in blend 1 (PS/PP/HDPE), A = PS, B = PP, and C = HDPE. The contact angles are  $\theta_A = \theta_{\text{PS}}$ ,  $\theta_B = \theta_{\text{PP}}$ , and  $\theta_C = \theta_{\text{HDPE}}$ . The interfacial tension ratios are  $\Gamma_A = \Gamma_{\text{PS}}$ ,  $\Gamma_B = \Gamma_{\text{PP}}$ , and  $\Gamma_C = \Gamma_{\text{HDPE}}$  (eqs 4a–4c), while the absolute interfacial tensions are  $\gamma_{\text{AB}} = \gamma_{\text{PS/PP}}$ ,  $\gamma_{\text{AC}} = \gamma_{\text{PS/HDPE}}$ , and  $\gamma_{\text{BC}} = \gamma_{\text{PP/HDPE}}$ . A similar identification procedure is used for the other blends.

Figure 2 shows the geometric construction used to determine the contact angles and the interfacial tensions ratios.<sup>24</sup> The AB, AC, and BC interfaces are first completed to full circles, and their origins are joined by a common segment defining the symmetrical axis of rotation. Following this, the origin of each circle is joined to the line of 3-phase contact by the radius of curvature  $r_{\text{AB}}$ ,  $r_{\text{AC}}$ , and  $r_{\text{BC}}$ . The angles  $\phi_{\text{AB}}$ ,  $\phi_{\text{AC}}$ , and  $\phi_{\text{BC}}$  are comprised by the axis of symmetry and the radius of curvature joining the circles' origins to the 3-phase line of contact. The contact angles  $\theta_A$ ,  $\theta_B$ , and  $\theta_C$  are calculated using the following equations:

$$\theta_A = \phi_{\text{AC}} + \pi - \phi_{\text{AB}} \quad (6a)$$

$$\theta_B = \phi_{\text{AB}} + \phi_{\text{BC}} \quad (6b)$$

$$\theta_C = \pi - \phi_{\text{AC}} - \phi_{\text{BC}} \quad (6c)$$

This approach was used because of the difficulty in directly tracing tangent lines at the 3-phase line of contact. Finally, knowing the  $\theta_i$  angles, the interfacial tension ratios  $\Gamma_i$  were calculated using eqs 4a–4c. Note that  $\phi_{\text{BC}}$  tends to zero and  $r_{\text{BC}}$  tends to infinity when phase C changes from a minor to a major phase, and eqs 6a–6c can then be simplified. This simplification has been used for blends 1, 3, 5, and 6. More details concerning the geometrical analysis are given in ref 24.

The number of measurements  $N$ , the average contact angles, and the associated standard deviations are given in Table 5 for

**Table 5. Number of Measurements  $N$ , Average Contact Angles, and the Corresponding Standard Deviations for Each Blend**

blend	no. of measurements $N$	$\theta_A$ (deg)	$\theta_B$ (deg)	$\theta_C$ (deg)
1	34	$171 \pm 6$	$48 \pm 12$	$141 \pm 10$
2	20	$44 \pm 8$	$150 \pm 7$	$166 \pm 5$
3	42	$144 \pm 7$	$78 \pm 11$	$139 \pm 10$
4	28	$161 \pm 9$	$172 \pm 4$	$30 \pm 9$
5	39	$165 \pm 9$	$107 \pm 10$	$88 \pm 12$

**Table 6. Average Interfacial Tension Ratios and Standard Deviations for  $\Gamma_A$ ,  $\Gamma_B$ , and  $\Gamma_C$  Obtained by the FIB-AFM-NT Method Compared with the Breaking Thread Method Results**

blend	FIB-AFM-NT			breaking thread		
	$\Gamma_A$	$\Gamma_B$	$\Gamma_C$	$\Gamma_A$	$\Gamma_B$	$\Gamma_C$
1	$1.2 \pm 0.1$	$0.3 \pm 0.15$	$0.2 \pm 0.1$	$1.4 \pm 0.3$	$0.5 \pm 0.3$	$0.39 \pm 0.15$
2	$2.2 \pm 0.5$	$3.0 \pm 0.5$	$1.4 \pm 0.1$	$1.5 \pm 0.2$	$2.4 \pm 0.2$	$1.7 \pm 0.5$
3	$1.5 \pm 0.2$	$0.9 \pm 0.2$	$0.6 \pm 0.1$			$0.41 \pm 0.15$
4	$0.4 \pm 0.15$	$0.7 \pm 0.2$	$2.1 \pm 1.1$	$0.5 \pm 0.1$	$0.7 \pm 0.1$	$1.5 \pm 0.3$
5	$0.95 \pm 0.05$	$0.3 \pm 0.15$	$0.3 \pm 0.15$			

each blend. The average interfacial tension ratios and the associated standard deviations are reported in Table 6. Finally, the ratios calculated with the breaking thread measurements are also reported in Table 6 for comparison purposes.

*2.7.2. Sensitivity Analysis of the NT Method.* A sensitivity analysis for the FIB-AFM-NT method was conducted in order to verify how much  $\Gamma$  varies for a small variation of  $\theta$ . The first partial derivatives of each interfacial tension ratio  $\Gamma_k(\theta_i, \theta_j)$  (eqs 4a–4c) were calculated for each blend. They are

$$\frac{\partial \Gamma_k}{\partial \theta_i} = \frac{\cos \theta_j \Delta \theta_i}{\sin \theta_j} \quad (7a)$$

$$\frac{\partial \Gamma_k}{\partial \theta_j} = \frac{-\cos \theta_i \sin \theta_i \Delta \theta_j}{(\sin \theta_j)^2} \quad (7b)$$

The sensitivity is calculated by using the quadrature of the two partial derivatives with the standard deviations  $\Delta \theta_i$  and  $\Delta \theta_j$  on the average experimental contact angles. In most cases, the calculated sensitivities are similar to the reported experimental errors on  $\Gamma_k$ . As expected,  $\Gamma$  varies rapidly when a contact angle is either near 0° or 180°. These tendencies are representative of the results presented in Tables 5 and 6.

*2.7.3. Contact Angle Values When the 3-Phase Contact Line Is Cut Nonperpendicularly.* During the FIB milling step, the line of

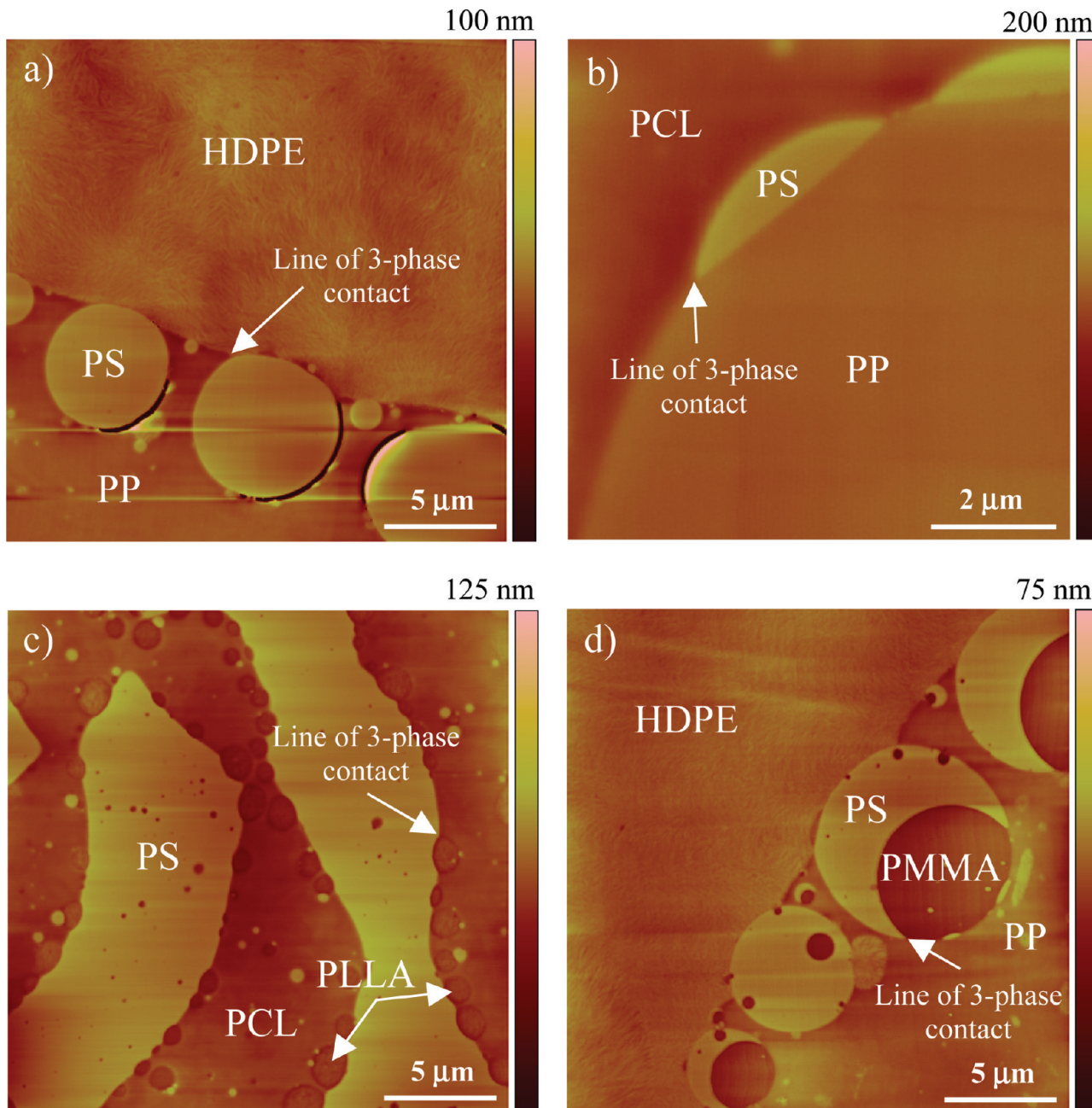


**Figure 4.** FIB-AFM topographical images of blends 1–4 displaying partial wetting between the components: (a) PS/PP/HDPE (blend 1), (b) PS/PCL/PP (blend 2), (c) PLLA/PCL/PS (blend 3), (d) PMMA/PP/PS/HDPE (blend 4).

3-phase contact is not necessarily cut perpendicularly and the measured contact angles are not the real ones, but apparent ones. An initial verification of this effect on the average  $\Gamma$  values was done by conducting a simple simulation with a system geometrically similar to blend 1, with a droplet of phase A at a planar BC interface. Initial values were assigned to the three interfacial tensions (similar to the experimental ones obtained for blend 1, with  $\gamma_{AC} = 4.2$ ,  $\gamma_{AB} = 3.5$ , and  $\gamma_{BC} = 1.1$  mN/m), and the three real contact angles and interfacial tension ratios for the simulated system were calculated.<sup>24</sup>

Following this, the simulated droplet was cut 67 times at different positions along the line of contact with varying orientations in order to calculate the average apparent contact angles and interfacial tension ratios. The results suggest that experimental measurements will, on average, yield interfacial tension ratios within 5–15% of their true values. Furthermore, the simulated standard deviations on average  $\theta$  and  $\Gamma$  values compare very well with the experimental standard deviations,

suggesting that the distributions around the average values come principally from this nonperpendicular cutting effect. More details on these results are given elsewhere.<sup>46</sup>

### 3. Results and Discussion

**3.1. Morphology after Quiescent Annealing.** Figure 4 shows the morphology of blends 1–4 after melt processing and 30 min of quiescent annealing time. As reported in a recent article from this group,<sup>36</sup> PS/PP/HDPE ternary blends display a partial wetting type of morphology with a 3-phase line of contact (Figure 4a). At a 10/45/45 vol % composition, the resulting morphology consists of PS droplets located at the HDPE/PP interface with a fraction remaining in the PP phase. The location of the PS droplets at the PP/HDPE interface is predicted by the three negative spreading coefficients (Table 4), and their affinity for the PP side of the PP/HDPE interface is expected since the PS/PP

interfacial tension is lower than the PS/HDPE one. Furthermore, it is relevant to note that the spreading coefficient  $\lambda_{\text{HDPE/PP/PS}}$  is only slightly negative. This may explain why PS droplets are also observed in the PP phase, since viscoelastic forces might be strong enough in that case to pull PS droplets into the PP phase during the melt processing step.

A similar result is obtained for the PS/PCL/PP 4/53/43 blend (blend 2, Figure 4b). PS droplets are observed at the PCL/PP interface, as predicted by the corresponding spreading coefficients (Table 4). In contrast, PLLA droplets are observed at the PCL/PS interface in the PLLA/PCL/PS 10/45/45 blend (blend 3, Figure 4c). The spreading coefficients could not be calculated in this latter case since there was no available data on the PLLA/PCL interfacial tension. However, it is reasonable to assume that this tension is relatively low since Sarazin et al.<sup>47</sup> have shown that PCL forms submicrometer droplets in a PLA matrix.

For the quaternary blend PMMA/PP/PS/HDPE (blend 4, Figure 4d), the analysis is more delicate since one set of three spreading coefficients is not enough to predict the resulting morphology. However, we can analyze the spreading coefficients of the four different ternary combinations in order to understand the resulting microstructure (Table 4). In ternary HDPE/PS/PMMA blends, complete wetting is theoretically predicted and experimentally observed, with the PS spreading at the HDPE/PMMA interface.<sup>20,31,32</sup> PMMA is then completely separated from the HDPE, as the schematics of Figure 1a,c illustrate. The spreading coefficients for the PMMA/PP/PS blend predict a partial wetting type of morphology. As a result, the minor phases of PS and PMMA dispersed in PP should give composite droplets of PS and PMMA, but with the two minor phases in contact with each other and the PP phase along a common line of contact, as the schematic of Figure 1d illustrates. For the PS/PP/HDPE combination, the PS is in contact with both the HDPE and the PP, as in blend 1 and as predicted by the corresponding spreading coefficients. Finally, for the PMMA/PP/HDPE ternary system,  $\lambda_{\text{HDPE/PP/PMMA}}$  is positive, which means that the PMMA should be completely separated from the HDPE by the PP phase. The FIB-AFM image of Figure 4d shows that all these tendencies are respected. The PMMA phase is completely separated from the HDPE and is in contact with the PS and the PP along a common line. In this case, the four sets of spreading coefficients support each other and seem to drive the morphology toward the equilibrium state. However, it is quite possible that other quaternary combinations could present conflicting sets of spreading coefficients, which would make the morphology analysis more delicate. Furthermore, more complex morphologies, not predicted by the spreading coefficients, could arise in quaternary blends such as the formation of a 4-phase line of contact.<sup>26–28</sup>

Finally, these results clearly show that partial wetting can be expected to be a frequently observed morphology in ternary and quaternary blends.

### 3.2. Measurement of the Interfacial Tensions Using the Neumann Triangle Method Combined with FIB and AFM.

**3.2.1. Unmodified Ternary and Quaternary Systems.** In a ternary system, partial wetting between the components is a necessary condition in order to use the Neumann triangle method to measure the interfacial tension ratios. As shown in the preceding section, blends 1–4 do satisfy this prerequisite. The Neumann triangle method was applied following the FIB-AFM-NT protocol described in section 2.7. Figure 5 and Figure 6 show examples of the geometric constructions used to measure the contact angles for the PS/PP/HDPE and PMMA/PP/PS ternary combinations (blends 1 and 4).

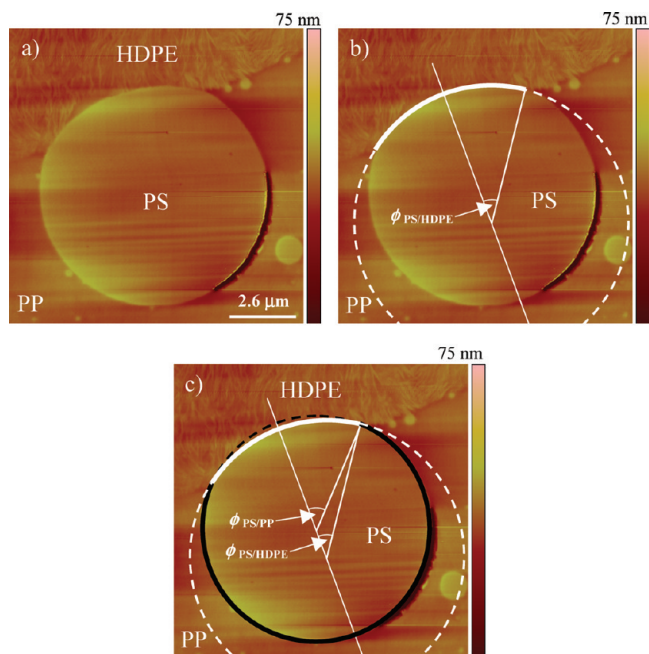


**Figure 5.** Example of the geometrical construction used to measure the interfacial tension ratios for the PS/PP/HDPE ternary blend (blend 1). (a) Original FIB-AFM image. (b) Circle fitted on the PS/HDPE interface (in white), with the corresponding angle  $\phi_{\text{PS/HDPE}}$  and radius of curvature  $r_{\text{PS/HDPE}}$  joining the circle's center to the line of 3-phase contact. (c) Addition of the circle fitted on the PS/PP interface (in black) with the corresponding angle  $\phi_{\text{PS/PP}}$  and radius of curvature  $r_{\text{PS/PP}}$  joining the circle's center to the line of 3-phase contact. Note that the PP/HDPE interface is planar, so that the angle  $\phi_{\text{PP/HDPE}} = 0$  and the radius of curvature  $r_{\text{PP/HDPE}} \rightarrow \infty$ .

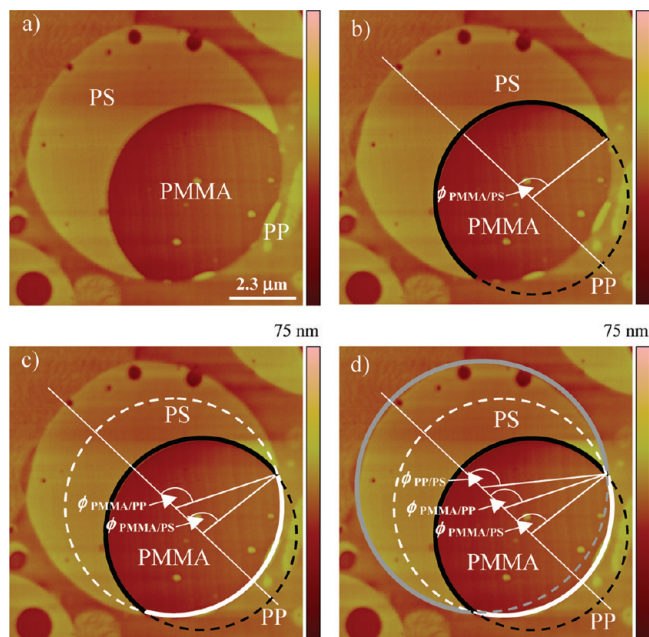


**Figure 6.** Example of the geometrical construction used to measure the interfacial tension ratios for the PMMA/PP/PS ternary combination in the PMMA/PP/PS/HDPE quaternary blend (blend 4). (a) Original FIB-AFM image. (b) Circle fitted on the PMMA/PS interface (in black), with the corresponding angle  $\phi_{\text{PMMA/PS}}$  and radius of curvature  $r_{\text{PMMA/PS}}$  joining the circle's center to the line of 3-phase contact. (c) Addition of the circle fitted on the PMMA/PP interface in white with the corresponding angle  $\phi_{\text{PMMA/PP}}$  and radius of curvature  $r_{\text{PMMA/PP}}$  joining the circle's center to the line of 3-phase contact. (d) Similar procedure for the PP/PS interface in gray.

The  $\phi_{ij}$  angles were measured manually with a precision of  $\pm 1^\circ$ , and the  $\theta_i$  angles were subsequently calculated using eqs 6a–c. The interfacial tension ratios  $\Gamma_A$ ,  $\Gamma_B$ , and  $\Gamma_C$ , as defined in eqs 4a–c, were calculated. For comparison purposes, the interfacial tension ratios were also calculated using the interfacial tensions measured with the breaking thread (BT) method. The number of measurements  $N$ , the average values, and the standard deviations of the interfacial tension ratios are reported in Table 5 and Table 6.

For the PS/PP/HDPE blend (blend 1),  $\Gamma_A = \Gamma_{PS} = \gamma_{PS/HDPE}/\gamma_{PS/PP}$ ,  $\Gamma_B = \Gamma_{PP} = \gamma_{PP/HDPE}/\gamma_{PS/PP}$ , and  $\Gamma_C = \Gamma_{HDPE} = \gamma_{PP/HDPE}/\gamma_{PS/HDPE}$ . The values in Table 6 obtained by the FIB-AFM-NT method compare very well with the results obtained with the breaking thread method. As pointed out in the Introduction, it is possible to calculate the absolute interfacial tension values from the ratios if at least one tension value out of three has been measured with another technique, such as the breaking thread. Using  $\gamma_{PP/PS} = 3.5 \pm 0.2$  mN/m ( $N = 5$ , Table 3) from the breaking thread technique results in  $\gamma_{PS/HDPE} = 4.2 \pm 0.6$  and  $\gamma_{PP/HDPE} = 1.1 \pm 0.6$  mN/m from the Neumann triangle approach. These latter values compare well with other reported values in the literature.<sup>18,20,21,31–33,43,44</sup> Note that it is important that accurate interfacial tension data be used to calculate the other two tensions using the Neumann triangle ratios.

The standard deviations for the results obtained by the FIB-AFM-NT method are between 0.1 and 0.15, while they are a little bit higher for the breaking thread method. In the case of very small interfacial tension ratios, as for  $\Gamma_{PP}$  and  $\Gamma_{HDPE}$ , the associated standard deviation becomes important when compared to the value of the interfacial tension. For the case of the breaking thread method, this comes primarily from the value of  $\gamma_{PP/HDPE}$  since the associated standard deviation is already large compared to the average value of the interfacial tension ( $\gamma_{PP/HDPE} = 1.9 \pm 0.5$  mN/m). In the case of the FIB-AFM-NT method, the error principally comes from the value of  $\sin \theta_{PS}$  ( $0.18 \pm 0.09$ ), since  $\theta_{PS}$  is close to  $170^\circ$ . It appears that for contact angles near  $180^\circ$  or  $0^\circ$  the standard deviations have a greater impact on the associated relative errors, while the absolute values are comparable.

Note that in some cases debonding between the PP and PS phases is observed. This is probably due to the contraction of the PP and HDPE phases when they recrystallize during quenching. However, this does not seem to affect significantly the curvature of the PS droplets (Figure 5). This debonding must be happening at a relatively low temperature ( $T_{\text{melting}}(\text{HDPE 3000}) \approx 120^\circ$  and  $T_{\text{melting}}(\text{PP PD702}) \approx 160^\circ$ ) so that the morphology is difficult to deform. Furthermore, measurements between particles exhibiting voids and those without voids show very similar results.

Blend 2 (PS/PCL/PP) also shows a good correlation between the interfacial tension ratios obtained from the Neumann triangle and the breaking thread methods in Table 6, although for the FIB-AFM-NT method,  $\Gamma_{PS} > \Gamma_{PP}$  ( $2.2 > 1.4$ ), while it is the opposite for the breaking thread with  $\Gamma_{PS} < \Gamma_{PP}$  ( $1.5 < 1.7$ ). Since  $\Gamma_{PS} = \gamma_{PS/PP}/\gamma_{PS/PCL}$  and  $\Gamma_{PP} = \gamma_{PCL/PP}/\gamma_{PS/PP}$ , this inversion could be due to an underestimated  $\gamma_{PS/PP}$  value using the breaking thread method (3.5 mN/m). With a value around 4.0 mN/m (more typically observed in the literature), this inversion disappears. This result clearly highlights the sensitivity of the analysis on the values of the interfacial tension ratios and therefore reinforces the need for an in situ measurement approach.

For blend 3 (PLLA/PCL/PS), the comparison between the Neumann triangle and the breaking thread method cannot be performed because  $\gamma_{\text{PLLA/PCL}}$  is unknown due to degrada-

tion issues during the BT experiment. To our knowledge, this interfacial tension value is not available in the literature. However, it is of great interest to see in Table 6 that the FIB-AFM-NT approach reveals that  $\gamma_{\text{PLLA/PCL}} = 2.7 \pm 1.3$  mN/m and  $\gamma_{\text{PLLA/PS}} = 4.0 \pm 1.7$  mN/m (5.8 mN/m by the BT) by using a value of  $\gamma_{\text{PCL/PS}} = 2.4 \pm 0.6$  mN/m ( $N = 7$ , BT value) with  $\Gamma_{\text{PCL}}$  and  $\Gamma_{\text{PS}}$ , respectively. Concern should be taken with regard to the possible degradation of the PLLA, even if quiescent annealing was performed for only 5 min. Furthermore, the question of whether or not local equilibrium along the 3-phase line of contact is reached after such a short time of annealing is addressed in a following section.

Finally, for the quaternary blend (blend 4, PMMA/PP/PS/HDPE), both the FIB-AFM-NT and the breaking thread methods in Table 6 give similar results. Using the FIB-AFM-NT method and a value of  $\gamma_{\text{PS/PP}} = 3.5 \pm 0.2$  mN/m (BT), it is found that  $\gamma_{\text{PMMA/PS}} = 1.7 \pm 1.0$  mN/m and  $\gamma_{\text{PMMA/PP}} = 5.0 \pm 0.8$  mN/m, which are comparable with the respective breaking thread values of  $2.4 \pm 0.3$  and  $5.7 \pm 1.5$  mN/m.

In summary, the NT and BT methods generally reveal the same overall trends; moreover, the interfacial tension ratios agree within the error margin except for the notable case of  $\Gamma_{\text{PS}}$  of blend 2. The Neumann triangle method combined with the FIB-AFM method thus seems sensitive enough to measure the interfacial tension ratios in melt-processed polymer blends when a partial wetting type of morphology is obtained. This approach could prove extremely useful when other methods are difficult to use, as in the case of the PLLA/PCL interfacial tension where polymer degradation is an issue. It allows, for the first time, the in situ measurement of the interfacial tensions of a blend system after melt processing using simple microstructural features. It would also be interesting to investigate the possibility of using this method when complex fluids are involved, like thermoplastic starch, liquid crystals, or for the case of solid/liquid solutions such as Pickering emulsions. Note that it is not expected that minor temperature variations would have a significant effect on these data since, as pointed out by Wu,<sup>48</sup> the temperature coefficient of interfacial tensions is usually smaller than  $-0.03$  mN/(m °C).

**3.2.2. Effect of the SEB Copolymer on the Morphology and the Interfacial Tension.** The addition of an SEB diblock copolymer to blend 1 (PS/PP/HDPE) significantly modifies the morphology and the geometry of contact between the phases. It decreases the PS/HDPE interfacial tension and displaces the PS droplets from the PP side to the middle or the HDPE side of the PP/HDPE interface (Figure 7). From a simple analysis based on the spreading coefficients, it has been shown recently that in order for the PS droplets to relocate on the HDPE side of the interface the HDPE/PS interfacial tension should decrease to a value between 3.5 and 1.6 mN/m.<sup>36</sup>

The Neumann triangle method is able to provide a more precise value of this modified interfacial tension in the compatibilized PS/PP/HDPE/SEB 10/45/45/(1% PS content) blend (blend 5, Table 2). In that case, the ratio  $\Gamma_{\text{PP}} = \gamma_{\text{PP/HDPE}}/\gamma_{\text{PS/PP}}$  has a value of  $0.3 \pm 0.15$  ( $N = 39$ ), equal to the value of the nonmodified system (blend 1). This result points toward two possibilities. The first is that both  $\gamma_{\text{PP/HDPE}}$  and  $\gamma_{\text{PS/PP}}$  are modified by the SEB copolymer in such a way that their ratio remains constant after modification. Although theoretically possible, this is unlikely at least for the HDPE/PP interface; the most probable conclusion is that both the PP/HDPE and PS/PP interfacial tensions are mostly unaffected by the copolymer.  $\Gamma_{\text{PS}}$ , however, decreases

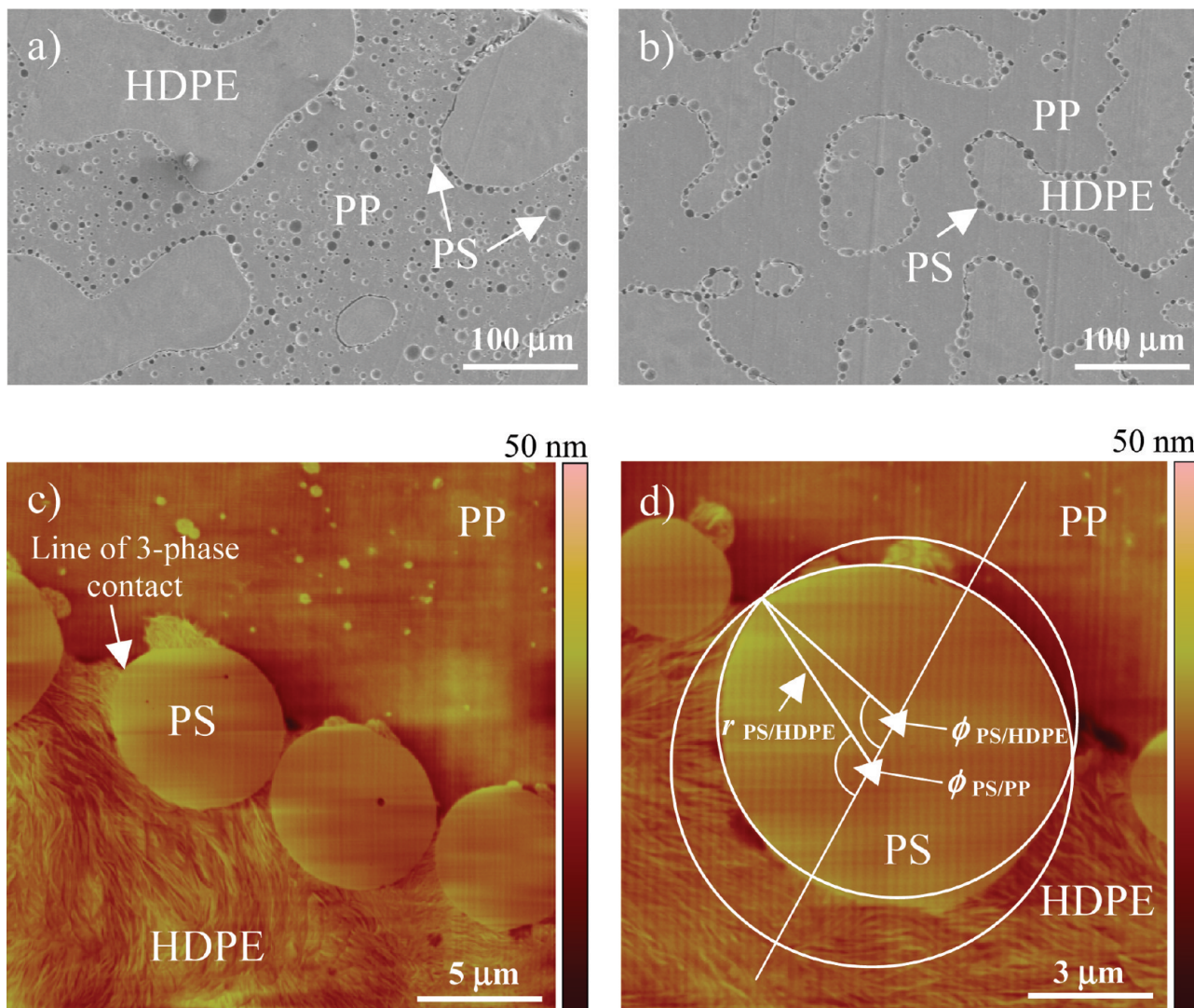


**Figure 7.** Effect of the SEB copolymer on PS/PP/HDPE ternary blend morphology. SEM micrograph of PS/PP/HDPE (a) with 0% SEB (PS extracted with cyclohexane) and (b) with 1% SEB based on the PS content (PS extracted with cyclohexane); (c) FIB-AFM image of the PS/PP/HDPE/SEB 10/45/(1% based on PS content) blend; (d) geometric construction on the FIB-AFM image to measure the  $\phi$  angles.

from  $1.2 \pm 0.1$  ( $N = 34$ , blend 1) to  $0.96 \pm 0.05$  ( $N = 39$ ) when the SEB compatibilizer is added to the blend. Since  $\gamma_{PS/PP}$  likely remains constant (from the analysis of  $\Gamma_{PP}$ ), this suggests that  $\gamma_{PS/HDPE}$  significantly decreases. Using these  $\Gamma_{PS}$  values and  $\gamma_{PS/PP} = 3.5 \pm 0.2$  mN/m (BT method),  $\Delta\gamma_{PS/HDPE} = -0.9 \pm 0.6$  mN/m and  $\gamma_{PS/HDPE}$  drops from  $4.2 \pm 0.6$  to  $3.3 \pm 0.4$  mN/m. We conclude that the addition of SEB in the blend induces a decrease of the PS/HDPE interfacial tension and is highly selective for the corresponding interface, having little effect on both the PP/HDPE and PS/PP interfaces.

For comparison purposes, Lepers and Favis<sup>49</sup> reported for a PS/EPR blend compatibilized with a similar SEB copolymer a drop in the interfacial tension from 6.5 to 3.4 mN/m using the breaking thread method. Mekhilef et al.<sup>43</sup> measured an interfacial tension decrease from 5.6 to 1.1 mN/m for an HDPE/PS blend with an SEBS triblock copolymer, while Elemans et al.<sup>44</sup> obtained a decrease from 4.7 to 1.1 mN/m for a PE/PS blend compatibilized with a diblock SEB. It is of interest to note that the interfacial tension decrease measured by Mekhilef et al.<sup>43</sup> ( $-4.5$  mN/m) and Elemans et al.<sup>44</sup> ( $-3.6$  mN/m) are significantly greater than the one we obtain ( $-0.9$  mN/m) by the Neumann triangle method. These discrepancies will be considered in detail in an upcoming paper.

It is also of interest to estimate the apparent areal density in copolymer at the HDPE/PS interface associated with the decrease of the interfacial tension. If all the copolymer is located at the HDPE/PS interface after melt processing and subsequent quiescent annealing, the apparent areal density  $\Sigma$  in copolymer can be calculated using the following formula:<sup>36</sup>

$$\Sigma = \frac{2r_{PS/HDPE}\phi_{\text{copo}}N_{\text{av}}}{3M_{\text{copo}}(1 - \cos \phi_{PS/HDPE})} \quad (8)$$

where  $r_{PS/HDPE}$  is the radius of curvature of the PS/HDPE interface,  $\phi_{\text{copo}}$  is the concentration of the copolymer in the PS phase,  $N_{\text{av}}$  is Avogadro's number,  $M_{\text{copo}}$  is the molecular weight of the copolymer, and  $\phi_{PS/HDPE}$  is the angle shown in Figure 7d. After 30 min of quiescent annealing time, the analysis of 12 droplets with an average radius of  $3.5 \pm 0.9$   $\mu\text{m}$  gives an average areal density of  $0.19 \pm 0.07$  copolymer molecules/ $\text{nm}^2$ , or  $5.0 \pm 1.5$   $\text{nm}^2$ /copolymer molecule, for a corresponding interfacial tension decrease of  $0.9 \pm 0.6$  mN/m.

This is an important result since it is still a challenge to measure the variation of the interfacial tension as a function of the copolymer areal density in multiphase polymer blends. Polizu et al.<sup>49</sup> and Cigana et al.<sup>51,52</sup> reported very similar areal density values at saturation of 0.18 molecule/ $\text{nm}^2$  in

**Table 7. Verification of the Laplace Equation with the Values Obtained by the Neumann Triangle Method**

blend	rhs of eq 11
1	1.02 ± 0.09
4	1.1 ± 0.2

PS/EPR blends compatibilized with an almost identical SEB diblock copolymer. Li et al.<sup>53</sup> showed comparable results for HDPE/PS blends compatibilized with SEB and SEBS copolymers. Macosko et al.<sup>54</sup> obtained a saturation value of 0.12 copolymer molecule/nm<sup>2</sup> for a deuterated PS-*block*-PMMA of  $M_n = 100\,900$ , and using a scaling law, they estimated the saturation value at 0.145 for a diblock of  $M_n = 55\,000$ . Adedeji et al.<sup>55</sup> reported apparent areal densities between 0.1 and 0.2 copolymer molecule/nm<sup>2</sup> for diblock PS-*b*-PMMA copolymers in binary blends of poly(cyclohexyl methacrylate) and poly(methyl methacrylate), near theoretical saturation values.

One of the advantages of the method we are presenting in this article is the possibility of measuring the variation of the interfacial tension as a function of added interfacial modifier, an issue that still poses challenges in the field of polymer blends. Although the breaking thread and pendant drop methods, for example, can report a decrease of the interfacial tension when a copolymer is added, it is difficult to estimate the amount of copolymer located at the interface since these are static or low-shear techniques in which the copolymer must preferentially be added to one of the two phases.<sup>43,44,49,56–59</sup> The approach we are proposing here allows for measurements of both the interfacial tension and the areal density of copolymer at the interface in situ in a melt-processed system. This significantly reduces the issues related to the migration of the modifier to the interface which limits the other techniques.

**3.2.3. Contact Angle Equilibrium after Quiescent Annealing.** In order for the Neumann triangle method to be applicable, viscoelastic, hydrodynamic, and inertial effects must be small or negligible compared to the effect of the interfacial tensions (or capillary effects) so that the system reaches a local quasi-equilibrium at the line of 3-phase contact. To evaluate the state of equilibrium of the system, it is of interest to look at the adimensional Bond number  $Bo$ , the capillary number  $Ca$ , and the capillary time  $\tau_c$ , defined by eqs 9a–9c:<sup>2</sup>

$$\text{Bond number : } Bo = \frac{\rho g R^2}{\gamma} \quad (9a)$$

$$\text{capillary number : } Ca = \eta_m \frac{\dot{\gamma} R}{\gamma} \quad (9b)$$

$$\text{capillary time : } \tau_c = \frac{\eta R}{\gamma} \quad (9c)$$

Here,  $\rho$  is the density of the droplet material,  $g$  is the gravitational acceleration,  $R$  is the radius of the droplet,  $\gamma$  is the interfacial tension,  $\eta_m$  and  $\eta_{DP}$  are the viscosities of the matrix and dispersed phases,  $\eta = (\eta_m \eta_{DP})^{1/2}$ , and  $\dot{\gamma}$  is the shear rate during quiescent annealing. The Bond number is a comparison between the inertial forces and the interfacial tension, while the capillary number is a comparison between the viscous forces and the interfacial tension. Finally, the capillary time is a characteristic time related to the relaxation of the system.

For a droplet of 10  $\mu\text{m}$  in diameter, with an interfacial tension around 3 mN/m and a density of about 1 g/cm<sup>3</sup>, the Bond number has a value of  $3 \times 10^{-5} \ll 1$ . This means that the capillary or interfacial forces are much stronger than the inertial forces and that the effect of gravity is negligible on the droplets we are investigating for all blends.

For the capillary number, the analysis is more delicate since there seems to be no available data on the shear rate in polymer blends during quiescent annealing. Using a viscosity of 1000 Pa s, an average interfacial tension of 3 mN/m, and a droplet radius of 3  $\mu\text{m}$ , the shear rate must be under 1 s<sup>-1</sup> in order to have a capillary number  $Ca < 1$  and under 0.1 s<sup>-1</sup> for a capillary number  $Ca < 0.1$ . The first case is when the viscous forces are of similar magnitude to the interfacial forces, while the second case is when the viscous forces are much smaller than the interfacial forces. Observation of our FIB-AFM micrographs shows that most of the droplets in the analyzed blends are nearly spherical or have interfaces with constant radius of curvature, and most show no sign of asymmetric deformation due to the flow field during quiescent annealing. This is a good indication that the viscous forces are relatively small and do not significantly affect the geometry of the droplets.

Finally, droplet relaxation after coalescence should be relatively fast and/or the frequency of collisions relatively low, in order to maximize the number of droplets at equilibrium in the analysis. In our case, using the same input parameters as for the determination of the Bond and Capillary numbers and  $\eta = 2000$  Pa s, we find  $\tau_{\text{cap}} \sim 10$  s. Using the quiescent annealing data for the PS/PP/HDPE blend in a recently submitted article,<sup>36</sup> we can calculate an approximate time required for the PS average droplet volume to double,  $\tau_{\text{double}}$ . The inverse of this characteristic time corresponds to an average coalescence frequency between PS droplets. After 30 min of quiescent annealing, the calculated frequency of coalescence between two PS droplets is about one process every 9 min (or 540 s), which is significantly above the calculated capillary time. This means that a PS droplet has more than enough time to relax to a quasi-equilibrium shape after merging with another one.

The Neumann triangle analysis should not be conducted on droplets having close neighbors in order to avoid significant deformation of the contact angles, and the image analysis should be conducted on droplets with constant interfacial radius of curvature. This last point is important and is a good indication of whether or not equilibrium is reached. If this condition is not met, the droplet is not at equilibrium. Coalescence between droplets and the effect of shearing during quiescent annealing are the principal factors affecting the equilibrium morphology necessary for the use of the Neumann triangle method.

**3.2.4. Using the Laplace Equation To Calculate Interfacial Tensions.** Another alternative approach to measure interfacial tension ratios is by using the Laplace equation. In this part of the work, we will apply it to blends 1 and 4, and it will be shown that the results are similar to those obtained with the Neumann triangle method.

In blends in which multiphase lines of contact are observed at equilibrium, two mechanical equilibrium conditions must be respected. The first one corresponds to the generalized Neumann triangle relation<sup>26–28</sup> at the line of contact between the phases. The second is the equality of the Laplace equation across each interface in the blend. As mentioned in the Introduction, in a ternary blend displaying partial wetting between phases A, B, and C (Figure 1d), the three Laplace equations that must be satisfied at equilibrium are given by eqs 2a–2c. They can be combined together to give the following relation:<sup>24</sup>

$$\frac{\gamma_{AB}}{r_{AB}} = \frac{\gamma_{BC}}{r_{BC}} + \frac{\gamma_{AC}}{r_{AC}} \quad (10)$$

where  $r_{AB}$ ,  $r_{BC}$ , and  $r_{AC}$  are the radius of curvature of the corresponding interfaces. When two interfacial tensions

and the radius of curvature of the interfaces are known, it is then possible to determine the third interfacial tension. Equation 10 can also be rearranged as follows:

$$1 = \left( \frac{\Gamma_A}{r_{AC}} + \frac{\Gamma_B}{r_{BC}} \right) r_{AB} \quad (11)$$

Table 7 reports the value of the right-hand side of eq 11 for blends 1 (PS/PP/HDPE) and 4 (PMMA/PP/PS/HDPE) using the  $\Gamma$  values obtained by the FIB-AFM-NT method. In both cases, the results are close to 1, thus satisfying eq 11. This shows that the Laplace equation can be used to calculate an interfacial tension ratio from eq 11 if the other is already known. Alternatively, using eq 10, one can calculate an interfacial tension, provided that two out of three tensions are already known.

The results presented in this paper are interesting in many ways. First, they show that it is possible to generate very complex morphologies with a relatively simple experimental approach combining mixing and quiescent annealing in order to let the equilibrium morphology develop. Furthermore, these structures can be used to obtain quantitative information on the state of the different interfaces, most notably the values of the interfacial tensions without and with interfacial modifiers. The apparent areal density of the copolymer can also be estimated. We are now currently investigating the effect of different copolymers on the resulting morphology and especially on the relative efficacy of interfacial modifiers. The methodology presented in this article could also be interesting to use for blends in which the interfaces are stabilized with solid particles.<sup>60–63</sup> In these systems, which are similar to Pickering emulsions, the solid particles tend to locate at the interfaces in order to minimize the interfacial energy. The contact angles at the 3-phase line that exists between the particles and the two homopolymers could be used to calculate the interfacial tension ratios. If the spatial resolution of the method proves sufficient, which for now is estimated to be somewhere between 10 and 50 nm, it could then be interesting to investigate the case of nanoparticles located at the interface. However, at this scale, the thermal energy of the particles might be comparable to the adsorption energy, leading to significant fluctuations of the contact angle values.

#### 4. Conclusion

We have used the Neumann triangle method (NT) in combination with a focused ion beam (FIB) sample preparation and atomic force microscopy analysis (AFM) to measure the interfacial tension ratios in ternary and quaternary polymer blends with and without the addition of an interfacial modifier. Ternary blends of PS/PP/HDPE, PS/PCL/PP, PLLA/PCL/PS, and PMMA/PP/PS and a quaternary blend of HDPE/PP/PS/PMMA all present a partial wetting type of morphology, a necessary condition for the Neumann triangle method to be applicable. The interfacial tension ratios obtained with the FIB-AFM-NT method compare well with those obtained by the classical breaking thread method (BT), and both the NT and BT techniques give similar relative magnitudes for the interfacial tensions. The addition of a small amount of an SEB diblock copolymer to the PS/PP/HDPE blend has a significant effect on the blend morphology. The FIB-AFM-NT method allows for the measurement of a modified PS/HDPE interfacial tension, going from  $4.2 \pm 0.6$  to  $3.3 \pm 0.4$  mN/m for an apparent areal density of  $0.19 \pm 0.07$  molecule/nm<sup>2</sup> in copolymer. This work opens new perspectives and approaches to generate complex morphologies and to quantify interfacial properties

between the blend components. It allows the measurement of the interfacial tension of a blend system examined in situ after melt processing from simple morphological features. This method can also provide important information concerning the influence of an interfacial modifier on the interfacial tension and morphology, which has been an important challenge in the polymer blend literature. Virtually all the classic techniques for the measurement of interfacial tension do not allow for the efficacious melt mixing of interfacial modifier in the blend system and its subsequent migration to the interface. This has been an important systemic weakness in those methods that this new approach is able to address. It also provides a route toward the measure of interfacial tension of systems that would otherwise experience degradation effects using typical ex situ approaches.

**Acknowledgment.** The authors gratefully acknowledge the financial support received from the Natural Sciences and Engineering Research Council of Canada (NSERC). N. Virgilio thanks the Fonds Québécois de la Recherche sur la Nature et les Technologies (FQRNT) for a scholarship and Dr. Pierre Sarazin for fruitful discussions.

#### References and Notes

- (1) Van Blaaderen, A. *Nature* **2006**, *439*, 545–546.
- (2) Fialkowski, M.; Bitner, A.; Grzybowski, B. A. *Nat. Mater.* **2005**, *4*, 93–97.
- (3) Ruzette, A.-V.; Leibler, L. *Nat. Mater.* **2005**, *4*, 19–31.
- (4) Roy, X.; Sarazin, P.; Favis, B. D. *Adv. Mater.* **2006**, *18*, 1015–1019.
- (5) Xing, P. X.; Bousmina, M.; Rodrigue, D.; Kamal, M. R. *Macromolecules* **2000**, *33*, 8020–8034.
- (6) Demarquette, N. R.; De Souza, A. M. C.; Palmer, G.; Macaubas, P. H. *Polym. Eng. Sci.* **2003**, *43*, 670–683.
- (7) Van Hemelrijck, E.; Van Puyvelde, P.; Macosko, C. W.; Moldenaers, P. J. *Rheol.* **2005**, *49*, 783–798.
- (8) Van Hemelrijck, E.; Van Puyvelde, P.; Velankar, S.; Macosko, C. W.; Moldenaers, P. J. *Rheol.* **2004**, *48*, 143–158.
- (9) Bousmina, M. *Rheol. Acta* **1999**, *38*, 73–83.
- (10) Jacobs, U.; Fahrlander, M.; Winterhalter, J.; Friedrich, C. *J. Rheol.* **1999**, *43*, 1495–1509.
- (11) Riemann, R. E.; Cantow, H. J.; Friedrich, C. *Macromolecules* **1997**, *30*, 5476–5484.
- (12) Riemann, R. E.; Cantow, H. J.; Friedrich, C. *Polym. Bull.* **1996**, *36*, 637–643.
- (13) Lacroix, C.; Bousmina, M.; Carreau, P. J.; Favis, B. D.; Michel, A. *Polymer* **1996**, *37*, 2939–2947.
- (14) Friedrich, C.; Gleinser, W.; Korat, E.; Maier, D.; Weese, J. *J. Rheol.* **1995**, *39*, 1411–1425.
- (15) Bousmina, M.; Bataille, P.; Sapieha, S.; Schreiber, H. P. *J. Rheol.* **1995**, *39*, 499–517.
- (16) Paliarne, J. F. *Rheol. Acta* **1990**, *29*, 204–214. Erratum: **1991**, *30*, 497.
- (17) De Freitas, C. A.; Valera, T. S.; De Souza, A. M. C.; Demarquette, N. R. *Macromol. Symp.* **2007**, *247*, 260–270.
- (18) Omonov, T. S.; Harrats, C.; Groeninckx, G. *Polymer* **2005**, *46*, 12322–12336.
- (19) Horiuchi, S.; Matchariyakul, N.; Yase, K.; Kitano, T. *Macromolecules* **1997**, *30*, 3664–3670.
- (20) Guo, H. F.; Packirisamy, S.; Gvozdic, N. V.; Meier, D. J. *Polymer* **1997**, *38*, 785–794.
- (21) Guo, H. F.; Gvozdic, N. V.; Meier, D. J. *Polymer* **1997**, *38*, 4915–4923.
- (22) Harkins, W. D.; Feldman, A. *J. Am. Chem. Soc.* **1922**, *44*, 2665–2685.
- (23) Harkins, W. D. *J. Chem. Phys.* **1941**, *9*, 552–568.
- (24) Torza, S.; Mason, S. G. *J. Colloid Interface Sci.* **1970**, *33*, 67–83.
- (25) Torza, S. *Interfacial Phenomena in Shear and Electrical Fields*. Ph.D. Thesis, McGill University, Montreal, **1969**.
- (26) Li, D.; Neumann, A. W. *Adv. Colloid Interface Sci.* **1994**, *49*, 147–195.
- (27) Chen, P.; Gaydos, J.; Neumann, A. W. *Langmuir* **1996**, *12*, 5956–5962.
- (28) Shadnam, M.; Amirfazli, A. *Langmuir* **2003**, *19*, 4658–4665.

- (29) Rowlinson, J. S.; Widom, B. In *Molecular Theory of Capillarity*; Dover Publications: Mineola, NY, 2002; p 327.
- (30) Hobbs, S. Y.; Dekkers, M. E. J.; Watkins, V. H. *Polymer* **1988**, *29*, 1598–1602.
- (31) Reignier, J.; Favis, B. D. *AIChE J.* **2003**, *49*, 1014–1023.
- (32) Reignier, J.; Favis, B. D.; Heuzey, M.-C. *Polymer* **2003**, *44*, 49–59.
- (33) Valera, T. S.; Morita, A. T.; Demarquette, N. R. *Macromolecules* **2006**, *39*, 2663–2675.
- (34) Zhang, J.; Ravati, S.; Virgilio, N.; Favis, B. D. *Macromolecules* **2007**, *40*, 8817–8820.
- (35) Debolt, M. A.; Robertson, R. E. *Polym. Eng. Sci.* **2006**, 385–396.
- (36) Virgilio, N.; Marc-Aurèle, C.; Favis, B. D. *Macromolecules* **2009**, *42*, 3405–3416.
- (37) Hyun, D. C.; Jeong, U.; Ryu, D. Y. *J. Polym. Sci., Part B: Polym. Phys.* **2007**, *45*, 2729–2738.
- (38) Kim, J. K.; Jeong, W.-Y.; Son, J.-M.; Jeon, H. K. *Macromolecules* **2000**, *33*, 9161–9165.
- (39) Zhang, X.; Kim, J. K. *Macromol. Rapid Commun.* **1998**, *19*, 499–504.
- (40) Virgilio, N.; Desjardins, P.; Pépin, M.-F.; L'Espérance, G.; Favis, B. D. *Macromolecules* **2005**, *38*, 2368.
- (41) Tomotika, S. *Proc. R. Soc. London, Ser. A* **1934**, *A150*, 322–337.
- (42) Utracki, L. A.; Shi, Z. H. *Polym. Eng. Sci.* **1992**, *32*, 1824–1833.
- (43) Mekhilef, N.; Favis, B. D.; Carreau, P. J. *J. Polym. Sci., Part B: Polym. Phys.* **1997**, *35*, 293–308.
- (44) Elemans, P. H. M.; Janssen, J. M. H.; Meijer, H. E. H. *J. Rheol.* **1990**, *34*, 1311–1325.
- (45) Biresaw, G.; Carriere, C. J. *J. Appl. Polym. Sci.* **2001**, *83*, 3145–3151.
- (46) Virgilio, N. Partial Wetting Phenomena in Ternary and Quaternary Immiscible Polymer Blends. Ph.D. Thesis, École Polytechnique de Montréal, Montréal, **2009**.
- (47) Sarazin, P.; Li, G.; Ortiz, W. J.; Favis, B. D. *Polymer* **2008**, *49*, 599–609.
- (48) Wu, S. In *Polymer Blends*; Paul, D. R., Newman, S., Eds.; Academic Press: New York, 1978; Vol. 1, p 268.
- (49) Lepers, J.-C.; Favis, B. D. *AIChE J.* **1999**, *45*, 887–895.
- (50) Polizu, S.; Favis, B. D.; Vu-Khanh, T. *Macromolecules* **1999**, *32*, 3448–3456.
- (51) Cigana, P.; Favis, B. D.; Jérôme, R. *J. Polym. Sci., Part B: Polym. Phys.* **1996**, *34*, 1691–1700.
- (52) Cigana, P.; Favis, B. D. *Polymer* **1998**, *39*, 3373–3378.
- (53) Li, J.; Favis, B. D. *Polymer* **2002**, *43*, 4935–4945.
- (54) Macosko, C. W.; Guégan, P.; Khandpur, A.; Nakayama, A.; Maréchal, P.; Inoue, T. *Macromolecules* **1996**, *29*, 5590–5598.
- (55) Adedeji, A.; Lyu, S.; Macosko, C. W. *Macromolecules* **2001**, *34*, 8663–8668.
- (56) Chang, K.; Macosko, C. W.; Morse, D. C. *Macromolecules* **2007**, *40*, 3819–3830.
- (57) Retsos, H.; Margiolaki, I.; Messaritaki, A.; Anastasiadis, S. H. *Macromolecules* **2001**, *34*, 5295–5305.
- (58) Hu, W.; Koberstein, J. T.; Lingelser, J. P.; Gallot, Y. *Macromolecules* **1995**, *28*, 5209–5214.
- (59) Anastasiadis, S. H.; Gancarz, I.; Koberstein, J. T. *Macromolecules* **1989**, *22*, 1449–1453.
- (60) Vermant, J.; Cioccolo, G.; Golapan Nair, K.; Moldenaers, P. *Rheol. Acta* **2004**, *43*, 529–538.
- (61) Mironi-Harpaz, I.; Narkis, M. *J. Appl. Polym. Sci.* **2001**, *81*, 104–115.
- (62) Calberg, C.; Blacher, S.; Gubbels, F.; Brouers, F.; Deltour, R.; Jérôme, R. *J. Phys. D: Appl. Phys.* **1999**, *32*, 1517–1525.
- (63) Gubbels, F.; Blacher, S.; Vanlathem, E.; Jérôme, R.; Deltour, R.; Brouers, F.; Teyssie, P. *Macromolecules* **1995**, *28*, 1559–1566.
- (64) Sarazin, P.; Favis, B. D. *Biomacromolecules* **2003**, *4*, 1669–1679.
- (65) Biresaw, G.; Carriere, C. J. *J. Polym. Sci., Part B: Polym. Phys.* **2002**, *40*, 2248–2258.